JOURNAL OF MATERIALS SCIENCE 30 (1995) 809–823

Surface modification of electrogalvanized steels by zinc phosphate conversion coatings

T. SUGAMA
Energy Efficiency and Conservation Division, Department of Applied Science, Brookhaven National Laboratory, Upton, NY 11973, USA

T. TAKAHASHI
Department of Inorganic Materials, Hyogo Prefectural Institute of Industrial Research, 3 Yukihira-cho, Suma-ku, Kobe 654, Japan

When electrogalvanized steel (EGS) surfaces were treated by immersing them in a phosphating solution consisting of $Zn_3(PO_4)_2 \cdot 4H_2O$, H_3PO_4, $Co(NO_3)_2 \cdot 6H_2O$, poly(acrylic acid) (p(AA)) and water, the resulting electrochemical reaction led to the creation of short-circuited cells with cobalt acting as the cathode and the galvanized (zinc) coating as the anode. These cells accelerate the anodic dissolution of zinc, which then rapidly precipitates embryonic zinc phosphate tetrahydrate (hopeite) crystals on the EGS surfaces, resulting in their complete coverage with fully grown hopeite crystals after only 5 s immersion. The hopeite layers formed not only serve to protect the galvanized coatings against NaCl-induced corrosion, but also contribute significantly to improving adhesion to the polyurethane (PU) topcoating. The reasons for the latter improvement were due primarily to the following: (1) the interfacial chemical reaction between the p(AA) existing at the top surface of hopeite and the PU, and (2) the anchoring effects of the penetration of PU into the rough hopeite crystal layers.

1. Introduction

In the automotive industries it is commonly known that electroplated coatings of pure zinc and various zinc alloys over steel surfaces are responsible for improving corrosion resistance by delaying the onset of "red rust" of body panels and various discrete parts, such as fasteners and brackets [1]. Pure zinc coatings currently have the major share of the automotive body-panel market. Although the art of making electroplated zinc coating for electrogalvanized coatings is well developed, two problem areas still remain. One is the poor adherence of galvanized (zinc) coating surfaces to the polymeric topcoats, and the other is the necessity of post-treatment to inhibit the onset of "white rust", which represents deterioration of the zinc layer. The former problem relating to the paint's adhesion properties is due primarily to the chemically inert, smooth texture of coating surfaces. One way to solve this problem is to increase the roughness of the surface either by etching or sand-blasting [2]. Such roughening procedures, which increase the actual surface area, provide more mechanical interlocking bonds at interfaces between the paint and the zinc coating. However, there is no resolution to inhibiting the onset of "white rust" of zinc layer.

Thus, our research focused on modifying zinc coating surfaces to improve their chemical and physical affinities with paint, and on retarding the corrosion rate of zinc layers. Poly(acrylic acid) (p(AA))-incorporated zinc phosphate solutions were used for the work. As discussed previously [3, 4], crystalline zinc phosphate (Zn·Ph) conversion castings can be prepared by immersing cold-rolled steel into a p(AA)-incorporated phosphating solution. The Zn·Ph coating deposited on the steel surfaces not only served to protect the underlying steel against corrosion, but also had excellent adherence to paint. The latter was due mainly to the combined effects of the very rough surfaces of Zn·Ph and the strong chemical affinities of p(AA) macromolecules existing at the top surface of the Zn·Ph layer. Our particular interests were in investigating how this phosphating solution is converted into solid Zn·Ph layers adhering to the underlying zinc coating, and how well the polymeric topcoat will bond to them. The studies centred on the liquid → solid phase transformation process, the morphological features and profiling analyses of Zn·Ph-covered electrogalvanized steel (EGS) structures, and adhesion in polymer film/Zn·Ph/EGS joint systems and their failure mechanism. In addition, we investigated the effect of cobalt ions incorporated in the phosphating bath on the rate of deposition of Zn·Ph on to EGS surfaces to obtain a fundamental understanding of the electrochemical activity of transition metals which promote conversion to the Zn·Ph phase.

0022–2461

2. Experimental procedure

2.1. Materials

The metal substrate used was ASE 1006 cold-rolled steel coated with electroplated zinc (Ford E 60 Electrozinc 60G), supplied by Advanced Coating Technologies, Inc. The formulation for the basic zinc-phosphate liquid was 4.7 wt% zinc orthophosphate tetrahydrate (Alfa Co.), 9.3 wt%H_3PO_4, 2.0 wt% 25% p(AA) colloidal solution (Rohm & Hass Co.), and 84.0 wt% water. The average molecular weight of the p(AA) was 60000. In modifying this standard formulation, $Co(NO_3)_2 \cdot 6H_2O$ added to the standard phosphating solution was 1.0 wt% of the total standard solution. The electroplated zinc-coated (galvanized) 1006 steels were immersed in the cobalt-modified and unmodified conversion solutions at 80 °C. Commercial-grade polyester-modified polyurethane (PU) M313 resin, supplied by the Lord Corporation, was used as an elastomeric topcoating. This PU contains a certain amount of silica as filler material. PU was polymerized by incorporating a 50 wt% aromatic amino curing agent, M201. The topcoat system then was cured in an oven at 80 °C.

2.2. Measurements

Scanning electron microscopy (SEM) with energy-dispersive X-ray spectrometry (EDX) was used to perform the image and elemental analyses of the coating surfaces, and to conduct the depth–composition profiling studies of Zn·Ph-deposited EGS. The phase identification and assemblage of Zn·Ph deposited on to EGS surfaces were examined by X-ray diffraction (XRD). We also investigated the chemical states and compositions at the outermost surface sites of the Zn·Ph-treated EGS, and on the bond-failure side at interfaces of the PU/Zn·Ph/EGS joint systems by combined X-ray photoelectron spectroscopy (XPS) and specular-reflectance fourier-transform infrared (SR–FT–IR) spectroscopy. Using XPS, the atomic concentrations of the respective chemical elements were estimated by comparing the XPS peak areas, which can be obtained from differential cross-sections for core-level excitation. To set a scale in the high-resolution XPS spectra, the binding energy (BE) was calibrated with C 1s of the principal hydrocarbon-type carbon peak fixed at 285.0 eV as an internal reference. A curve deconvolution technique, using a DuPont curve resolver, revealed the respective chemical components from the high-resolution spectra of each element.

The concentration of zinc ion dissociated from the EGS surfaces in a single H_3PO_4 and $Co(NO_3)_2 \cdot 6H_2O$ aqueous solution, and in their combined media, was determined by atomic absorption spectrophotometry (AA).

Electrochemical testing for corrosion was performed with the EG&G Princeton Applied Research Model 362-1 Corrosion Measurement System. The electrolyte was a 0.5 M sodium chloride solution, made from distilled water and reagent-grade salt. The specimen was mounted in a holder, and then inserted into an EG&G Model K47 electrochemical cell. The tests were conducted in an aerated 0.5 M NaCl solution at 25 °C, on an exposed surface area of 1.0 cm^2. The polarization curves containing the cathodic and anodic regions were measured at a scan rate of 0.5 mV s^{-1} in the corrosion potential range of −1.35 to −0.75 V. The salt-spray testing of Zn·Ph-coated EGS panels (75 × 75 mm) was performed in accordance with ASTM B 117.

Peel-strength tests of adhesive bonds at the polyurethane topcoat-modified EGS substrate interfaces were conducted at a separation angle of ≈180° and a crosshead speed of 5 cm min^{-1}. The specimens consisted of one piece of flexible or rigid substrate material, 2.5 cm × 20.3 cm, with the unbounded portions of each member being face-to-face. The thickness of the PU topcoat overlaid on the Zn·Ph surfaces was ≈0.95 mm.

3. Results and discussion

3.1. Zinc phosphate-treated EGS surfaces

Figs 1 and 2 are scanning electron micrographs of crystalline Zn·Ph coatings derived from the unmodified and $Co(NO_3)_2 \cdot 6H_2O$-modified phosphating solutions, respectively, as a function of the length of immersion time of the EGS substrate in the phosphating bath at 80 °C. Using the unmodified solution, the precipitation of rectangular-shaped Zn·Ph crystals on the EGS surfaces occurred slowly. The SEM image of specimens made after immersion for 1 min revealed a random distribution of rectangular Zn·Ph crystals over the EGS (Fig. 1a). Increasing immersion to 5 min (Fig. 1b) led to extensive coverage of Zn·Ph on the EGS, while the crystal size increased remarkably. Complete coverage of fully grown crystals was attained after immersion for 30 min (Fig. 1d). In contrast, the $Co(NO_3)_2 \cdot 6H_2O$-modified solution was quite effective in causing rapid deposition of the Zn·Ph layers. Fig. 2 shows that the growth of lamellar-like crystals was observed after immersion for only 2 s (b), compared with the surface texture of the 1 s-treated EGS (a). Immersion for 5 s was sufficient to produce dense conversion coatings over the entire substrate surface (see Fig. 2c). A further extension of immersion to 10 s (d) revealed a densely packed conformation of lamellar Zn·Ph crystals, reflecting that the EGS surface had essentially been altered and now had a rough microstructure. Note that the morphological and topographical characteristics of this crystal were quite different from those of the crystal layers induced by the unmodified solution.

As a result of these findings we turned our attention to exploring how well the cobalt-modified Zn·Ph coatings adhere to the underlying EGSs, and how the zinc layers were damaged by the phosphating solution. We examined the cross-sections through the Zn·Ph-treated and untreated EGS surfaces by SEM and EDX (Fig. 3). The SEM image of the "as-received" EGS (a) showed that the electroplated zinc layer denoted as the "2" layer has a thickness of ≈10 μm. The layer denoted "1" is the underlying steel layer. As seen on the EDX spectrum (d) of "2", there is some iron in this porous zinc layer. Because the source

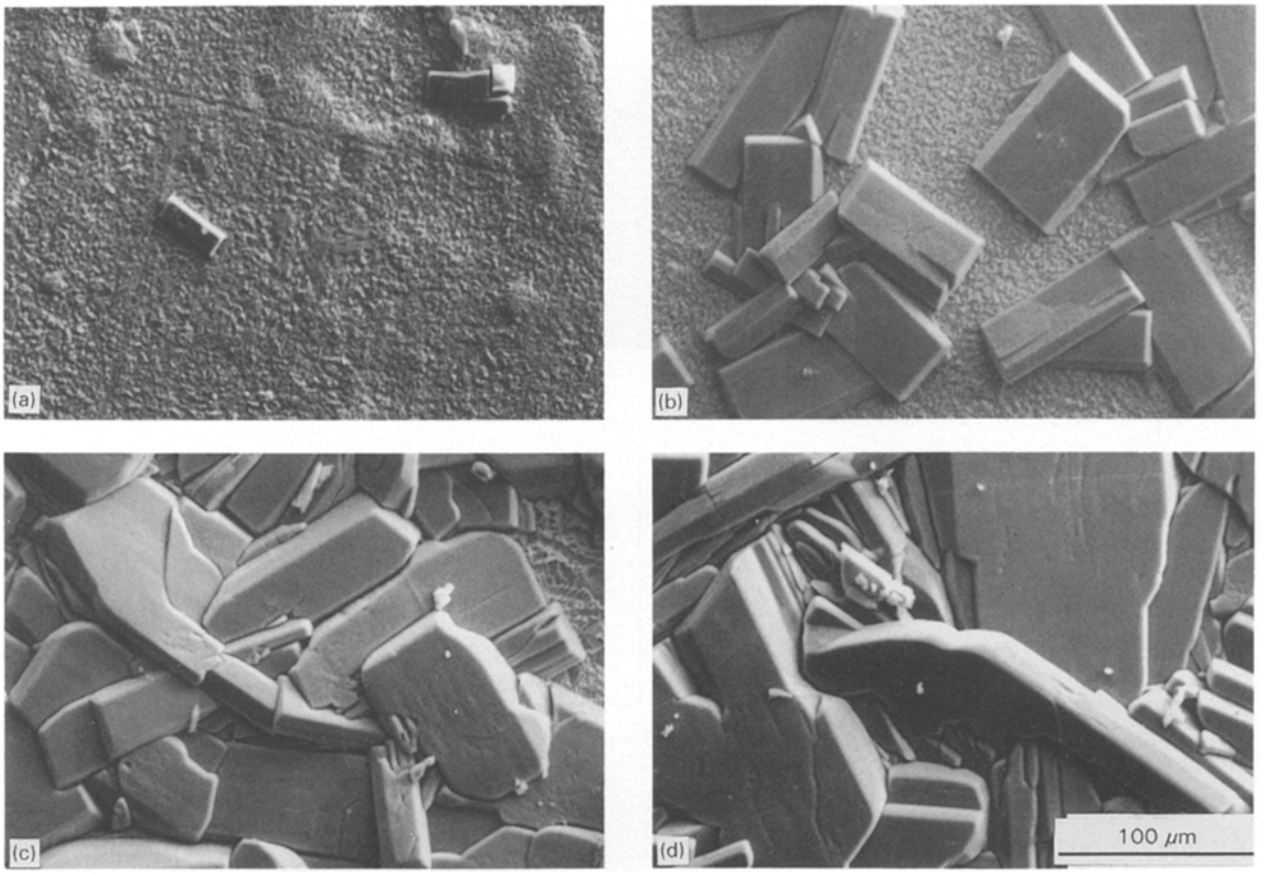

Figure 1 Scanning electron micrographs of Zn·Ph crystals derived from unmodified phosphating solution by varying the immersion times: (a) 1 min; (b) 5 min; (c) 20 min; (d) 30 min.

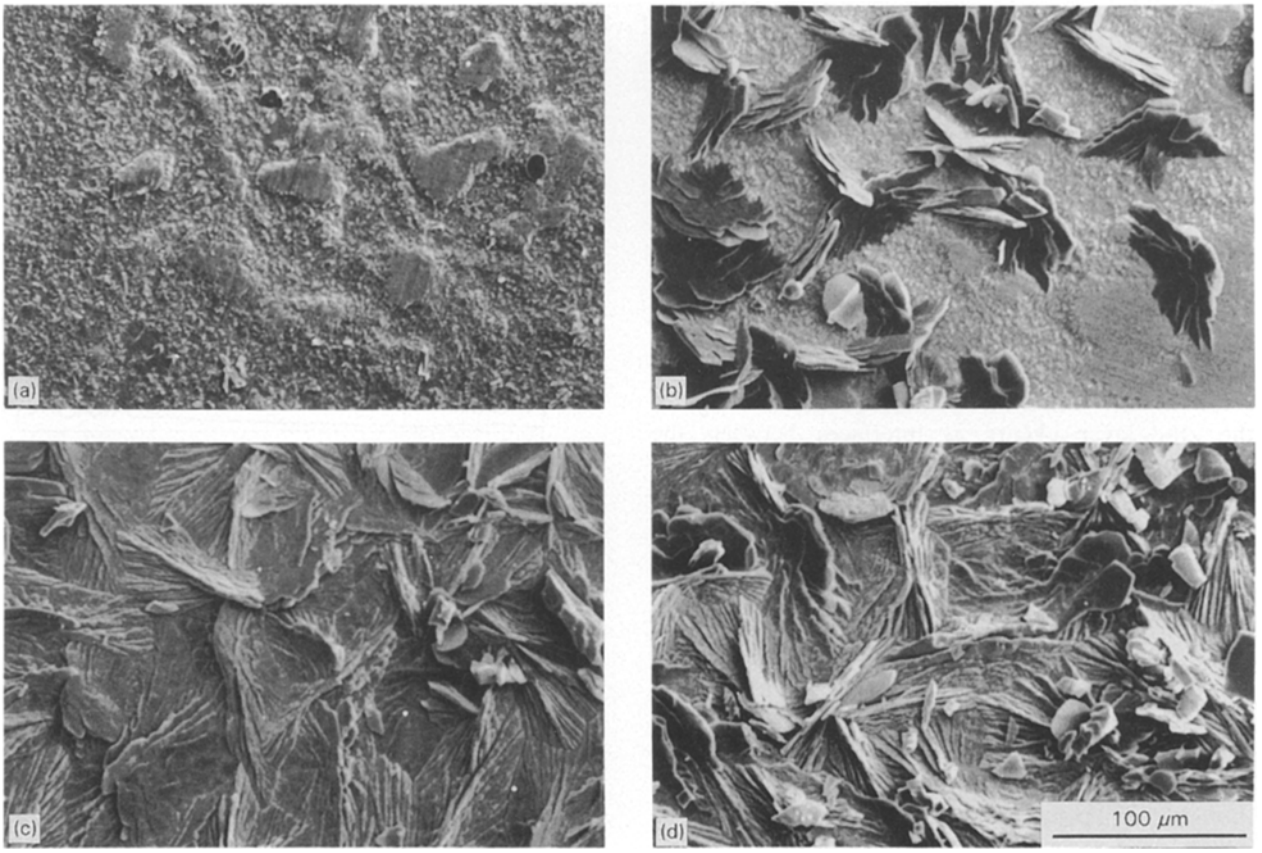

Figure 2 SEM images of cobalt-modified Zn·Ph deposited rapidly on EGS surfaces, after immersion for (a) 1 s; (b) 2 s; (c) 5 s; (d) 10 s.

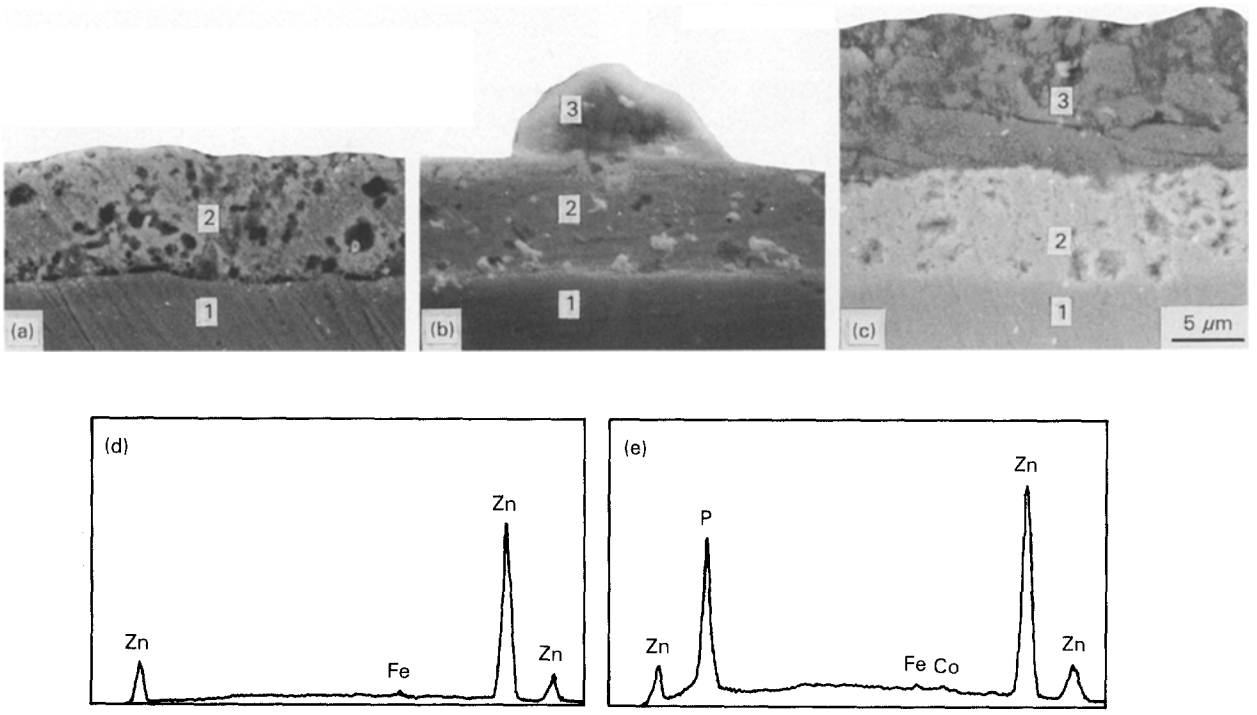

Figure 3 SEM–EDX examinations of cross-section through (a) the "as-received" EGS and (b) 2 s and (c) 10 s treated cobalt-modified Zn·Ph surfaces.

of iron is the steel, iron had migrated from the steel to the matrix of pure zinc during the electroplating processes. Fig. 3b is an SEM image of a cross-section through the 2 s-treated cobolt-modified Zn·Ph surface. By comparison with that of the "as-received" EGS, the image indicates that an additional phase, denoted "3", is superimposed on the EGS surfaces. The EDX spectra of this superimposed layer showed the presence of zinc and phosphorus as principal components, and iron and cobalt as minor ones. Because zinc, phosphorus and cobalt reflect the formation of cobalt-modified Zn·Ph, it is apparent that the partial deposition of cobalt-modified Zn·Ph on to EGS occurs in the first 2 s of immersion. Complete coverage of modified Zn·Ph layer of ≈ 12 μm thick is recognizable on the SEM image of specimens after immersion for 10 s. The image also suggested that the thickness of the zinc layer was reduced from ≈ 10 μm in the original phase to ≈ 8 μm. Such a decrease may be due to its dissolution caused by the attack of phosphating solution on EGS surfaces. Although this damage to the zinc layer occurs at interfaces between the Co–Zn·Ph and EGS, no layer separation and segregation was observed in close examination of SEM images in the Zn·Ph–Zn boundary regions (not shown). This finding strongly suggested that the adhesive bond of Zn·Ph to zinc is good.

Fig. 4 illustrates the XRD tracing, ranging from 0.444–0.225 nm, of the "as received" EGS as a control, and the cobalt-modified Zn·Ph coatings prepared by immersing EGS panels for 1, 2, 5, and 10 s. The XRD pattern of the control shows the presence of a single phase only corresponding to the pure zinc crystal. Although the intensity of the XRD line is very weak, the Zn·Ph conversion products formed on EGS after immersing for 1 s can be identified as the hopeite, $Zn_3(PO_4)_2 \cdot 4H_2O$, phase. The intensity of these

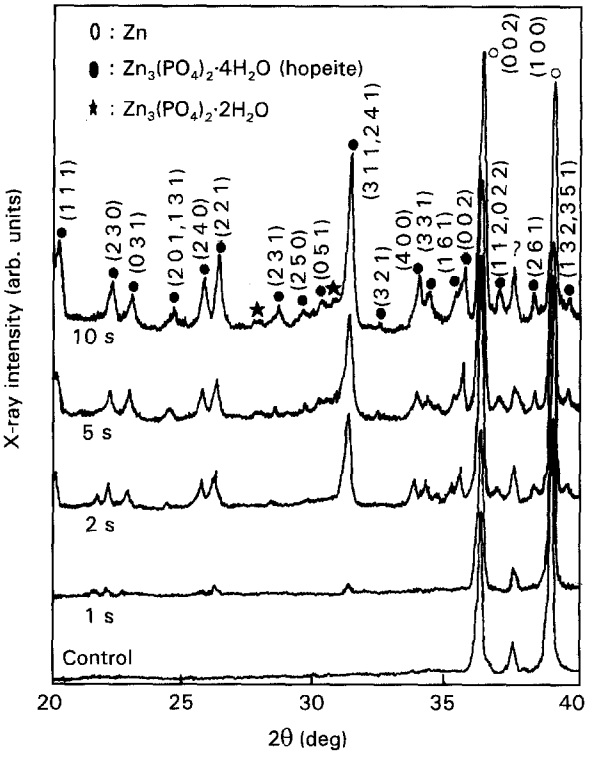

Figure 4 XRD patterns of "as-received" EGS surfaces as control, and cobalt-modified Zn·Ph made after immersion for 1, 2, 5 and 10 s.

hopeite lines markedly increased with increased immersion, while the strong lines of the underlying zinc phase are still present in the pattern. The data also indicated that zinc orthophosphate dihydrate, $Zn_3(PO_4)_2 \cdot 2H_2O$, coexists as minor phase with the hopeite. Similar phase compositions were identified from the unmodified Zn·Ph coatings prepared by immersing for 30 min; namely, the conversion coatings consisted of the hopeite as the principal and $Zn_3(PO_4)_2 \cdot 2H_2O$ as the minor one phase.

Next, using XPS, we investigated the changes in chemical composition of the surface of unmodified and cobalt-modified Zn·Ph coatings as a function of immersion time. These results are summarized in Table I. For the "as-received" EGS (control), the principal elements occupying the outermost surface sites were carbon and oxygen, and the concentration of zinc was 14.0%. Assuming that carbon reflects the presence of organic contaminants, the zinc and oxygen atoms presumably correspond to the formation of zinc oxide as the passivated film on EGS surfaces. Such films retard the precipitation of embryonic Zn·Ph crystals on EGS. In fact, using the unmodified phosphating solution, there was only 0.9% phosphorus in the first 60 s of immersion. Even when the immersion period was prolonged to 300 s there was no significant change in the phosphorus concentration. This verified that the passivating layer of ZnO inhibits the precipitation of Zn·Ph. Breakage of this passive film seemed to occur when the EGS was immersed for 600 s because of markedly increased phosphorus concentration; thus, a phosphorus content of 7.2%, corresponding to a P/Zn ratio of 0.6, was reported after 1800 s immersion. Note that the source of carbon for all phosphated EGS specimens was not solely through contamination, but also from carbon in p(AA) absorbed by the EGS and Zn·Ph surfaces during the conversion reaction. Oxygen, ranging from 38.0%–50.1%, for the treated EGSs, is attributable to multiple compounds such as ZnO, Zn·Ph, organic contaminants, and p(AA).

Using the $Co(NO_3)_2 \cdot 6H_2O$-incorporated phosphating solution, immersion of only 5 s resulted in the formation of conversion coatings having > 10.0% P, but beyond this time the phosphorus concentration levels off. This information directly supports the findings from the previous SEM image analysis, namely, Zn·Ph totally covers the EGS after ≈5 s. The data also indicated that the P/Zn ratio of the Co– Zn·Ph coating resulting from 5 s immersion is much higher than that from 1800 s immersion in unmodified Zn·Ph, implying that the Zn·Ph coating from the $Co(NO_3)_2 \cdot 6H_2O$-incorporated solution has a phosphorus-enriched surface layer.

Figs 5 and 6 show the high-resolution XPS spectra of P 2p, Zn 2p3/2 and C1s core-level excitations for the Co–Zn·Ph coatings as a function of treatment time. In the P 2p region (Fig. 5) no peak was found on the "as-received" EGS surfaces denoted "0 s". The coating made by 1 s dipping (1 s) exhibited two weak peaks, at 133.9 and 132.4 eV. The former presumably reveals the phosphorus originating from the Zn·Ph [5], and the latter may be due to the formation of zinc dihydrogen orthophosphate, $Zn(H_2PO_4)_2 \cdot xH_2O$ salt [6]. The peak intensity at 133.9 eV markedly increased with increased treatment time, while the peak at 132.4 eV vanished. The degree of coverage of Zn·Ph over EGS can be confirmed by comparing the spectral features of the Zn 2p3/2 region (Fig. 5). The single peak at the BE position of 1022.2 eV for the "as-received" EGS (0 s) is due to zinc in the ZnO layers [7, 8] forming on the top surface of the galvanized coatings. The Zn 2p3/2 curve of the 2 s-treated specimens (2 s) is distinctive; an additional weak line at 1023.0 eV appears in the spectrum, separate from the main line. The intensity of this new line dramatically increased as treatment was prolonged. After 5 s this peak eventually became the principal line, while the line at 1022.2 eV, originating from the zinc in ZnO, disappeared. Because the peak at 1023.0 eV belongs to zinc originating from Zn·Ph [3] this result strongly supported the SEM data showing that immersion for 5 s is long enough to cover the whole surface of EGS with Zn·Ph. The C 1s region of the untreated EGS surfaces (Fig. 6 (0 s)) had a symmetrical peak at 285.0 eV, reflecting the carbon in the hydrocarbon, "CH_n", contaminant. When this EGS surface was treated with a phosphating solution for 2 s the C 1s spectrum (2 s) revealed that the two resolvable Gaussian components at 285.0 eV as the principal components is not only attributable to hydrocarbon in the organic contaminant, but also to that in the backbone chain of p(AA). A second peak emerging at 288.7 eV corresponds to carbon originating from the carboxylic acid, COOH, in the p(AA) [9]. Increasing the treatment time to 10 s showed the emergence of an additional peak at 287.2 eV in the spectrum (10 s). We assigned this additional peak, emerging at the BE location between a carbonyl carbon, C=O, at ≈288.0 eV and a C–O single bond at ≈286.5 eV [10], to the carbon in the $-COO^-$–Zn^{2+}–OOC– salt complex formation [11, 12]. Nevertheless, both the bulk and complexed p(AA) polymers appear to be present at the outermost surface site of cobalt-modified Zn·Ph. Note that although the deposition of Zn·Ph is very poor, the presence of p(AA) was also identified on the EGS surfaces after immersion for 60 s in the phosphating solution without $Co(NO_3)_2 \cdot 6H_2O$, by XPS (not shown). Thus, p(AA) favourably diffuses to the ZnO surfaces.

An important question remains to be solved, namely, why the $Co(NO_3)_2 \cdot 6H_2O$-incorporated solution causes the rapid deposition of Zn·Ph on the EGS surfaces. To investigate the electrochemical activity of the $Co(NO_3)_2 \cdot 6H_2O$ reagent in the increase in the conversion rate of Zn·Ph, we used three solutions without the $Zn_3(PO_4)_2 \cdot 4H_2O$ and p(AA) reagents: (1) 10.0 wt%H_3PO_4–90.0 wt% water: (2) 1.2 wt%Co$(NO_3)_2 \cdot 6H_2O$–98.8 wt% water: and (3) 10.0 wt% H_3PO_4–1.2 wt%$Co(NO_3)_2 \cdot 6H_2O$–88.8 wt % water.

TABLE I Changes in atomic composition and ratio of EGS surface as a function of immersion time in cobalt-modified and unmodified zinc phosphating solutions

Solution	Time (s)	Atomic concentration (%)				
		P	C	O	Zn	P/Zn
Control	–	–	46.6	39.4	14.0	0.0
Unmodified	60	0.9	49.7	38.0	11.4	0.1
	300	1.1	37.3	50.1	11.5	0.1
	600	4.7	35.4	42.1	17.8	0.3
	1200	6.9	37.2	43.1	12.8	0.5
	1800	7.2	33.6	48.0	11.2	0.6
Cobalt-modified	1	1.2	57.7	30.8	10.3	0.1
	2	3.7	29.6	49.5	17.2	0.2
	5	12.0	20.5	60.6	6.9	1.7
	10	11.9	21.6	57.2	9.3	1.3

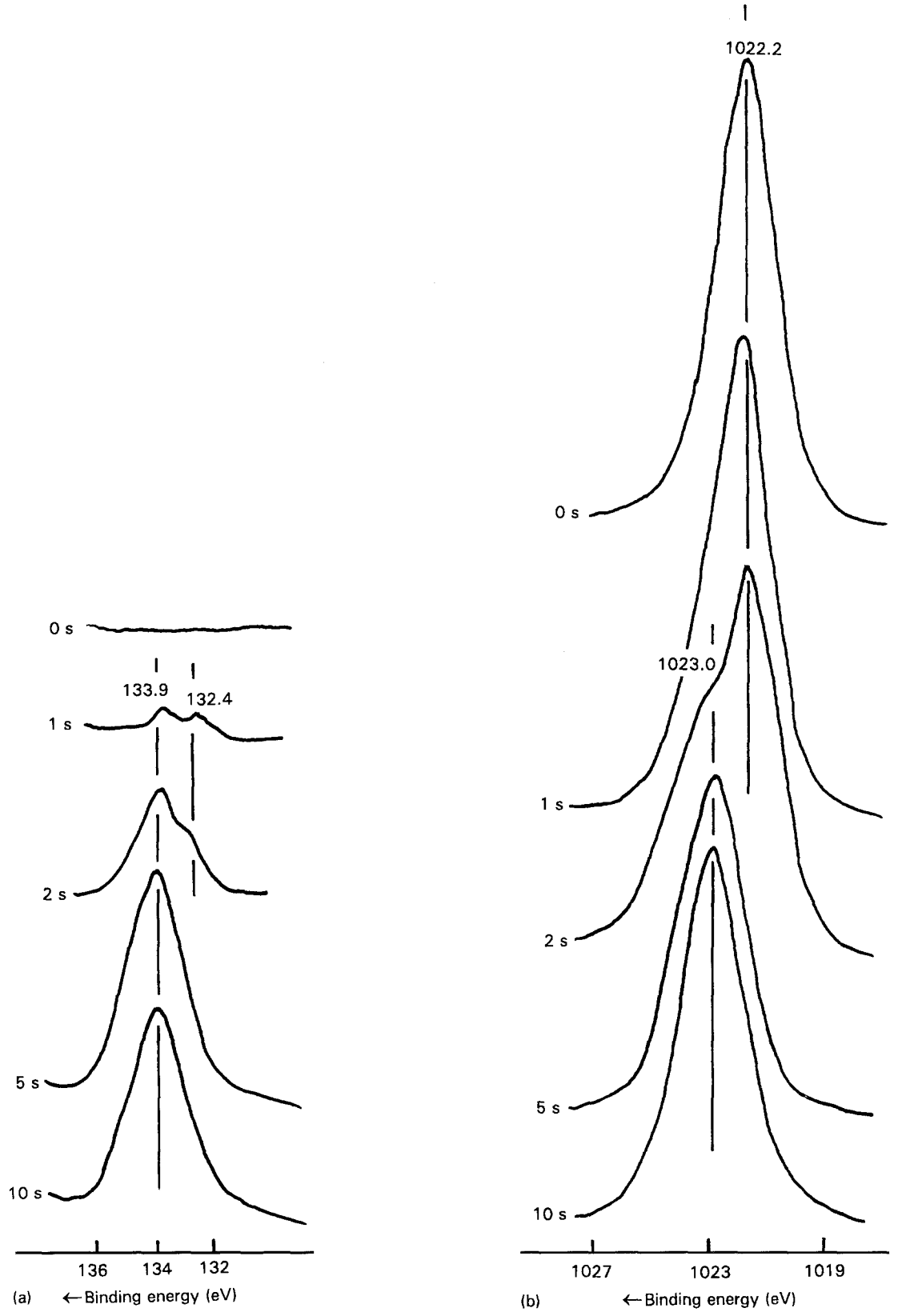

Figure 5 XPS (a) P_{2p} and (b) $Zn_{2p3/2}$ regions of cobalt-modified Zn·Ph deposited on EGS as a function of immersion time.

The experimental work was performed in accordance with the following sequence. First, an EGS test panel with a surface area of 100 cm^2 was immersed for 2, 5, 10, or 30 s, in a bath containing 1 l of these solutions at 80 °C. After withdrawing the panel the concentration of Zn ion in the bath was detected by A.A to gain the information on the anodic dissolution of the zinc coating. Fig. 7 shows the resulting dissolution rates, $\mu g\,ml^{-1}$, of zinc ions from the zinc coating, as a function of immersion times. When the EGS panels were soaked in the single $Co(NO_3)_2 \cdot 6H_2O$ solution, $\approx 4.6 \times 10^{-4}\ \mu g\,ml^{-1}$ of zinc ions dissociate from the EGS surfaces in the first 2 s of immersion; thereafter, the rate of zinc ion dissolution increases with increased time. The concentration of dissociated zinc ion after 30 s immersion was $\approx 2.8 \times 10^{-3}\ \mu g\,ml^{-1}$.

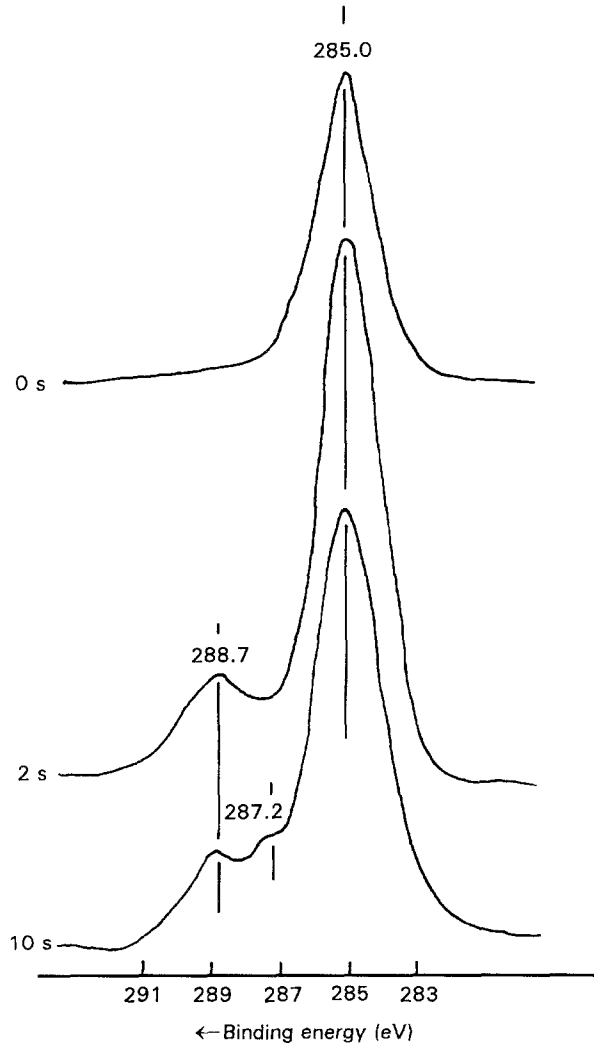

Figure 6 C_{1s} region of "as-received" EGS (0 s), and 2 s and 10 s-treated cobalt-modified Zn·Ph surfaces.

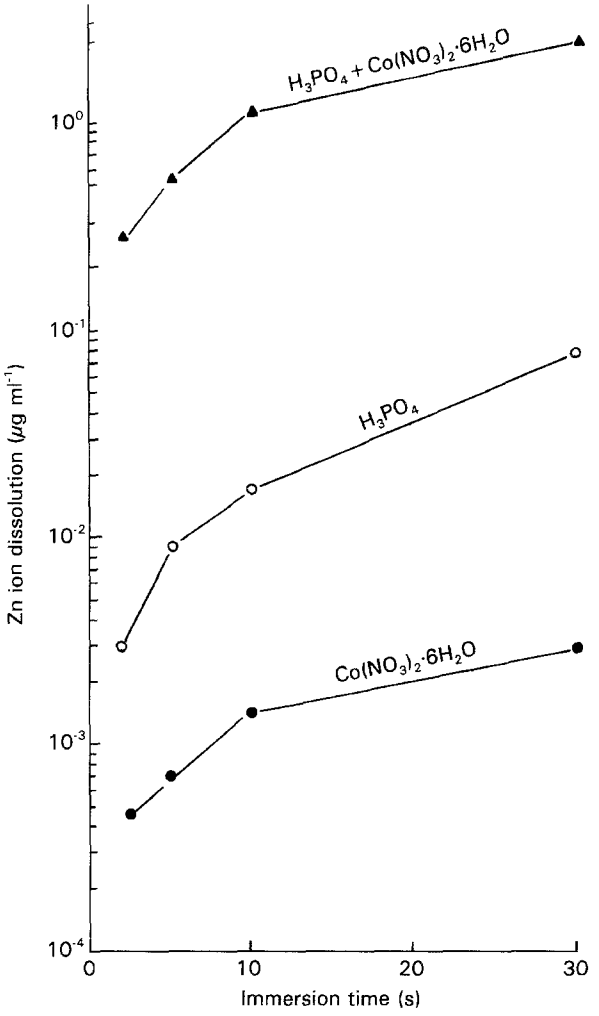

Figure 7 Changes in the concentration of zinc ions dissolved anodically from galvanized coating after immersion of EGS into H_3PO_4, $Co(NO_3)_2 \cdot 6H_2O$, and $H_3PO_4 + Co(NO_3)_2 \cdot 6H_2O$ solutions, respectively, at 80 °C.

Using the other single H_3PO_4 solution, the amount of Zn dissociated in 2–30 s corresponded to a tenfold increase over that of the $Co(NO_3)_2 \cdot 6H_2O$ solution. By comparison, a considerable volume of zinc ions was recorded from the combined solution of $Co(NO_3)_2 \cdot 6H_2O$ and H_3PO_4; immersion for only 2 s resulted in the dissociation of an abundance of zinc ions of near 1×10^{-1} μg ml^{-1}, and subsequently an increase in immersion to 30 s referred to the dissolution of 1.2 μg ml^{-1}. In addition, the extent of hydrogen evolution which was observed by the bubbling of the phosphating solution surrounding the EGS panel was in the following order: $H_3PO_4 + Co(NO_3)_2 \cdot 6H_2O \gg H_3PO_4 > Co(NO_3)_2 \cdot 6H_2O$ solutions. These findings verified that the addition of $Co(NO_3)_2 \cdot 6H_2O$ to H_3PO_4 solution significantly promotes the dissolution of zinc ions from the EGS surfaces in conjunction with a brisker evolution of hydrogen. A possible interpretation of the electrolytic corrosion of zinc layers in the H_3PO_4 electrolyte containing Co^{2+} ions is as follows: the electrochemical reaction between zinc and H_3PO_4 leads to the anodic dissolution of zinc, $Zn \rightarrow Zn^{2+} + 2e^-$, which is directly related to the corrosion of galvanized coatings. After the ejection of zinc ions, the $2e^-$ electrons generated by the anodic reaction of zinc preferentially react with the Co^{2+} ions dissociated from the $Co(NO_3)_2 \cdot 6H_2O$ reagents. This reaction can be described as the electron-trapping reaction, $Co^{2+} + 2e^- \rightarrow Co^\circ$ [13]. The elemental cobalt which is less electropositive than zinc may adhere to the zinc to create short-circuited cells, with zinc acting as the anodic area and cobalt as the cathode. Assuming that the creation of such a short-circuited cell is reasonable, the reaction of zinc with H_3PO_4 might be accelerated by the presence of a cathodic cobalt electrode. Once the dissolution of zinc ions has occurred in the anodic area, the electrons pass from zinc to cobalt, and then the uptake of electrons by hydrogen ions discharged from H_3PO_4 results in brisker evolution of hydrogen from the cathodic cobalt side:

$$2H_3PO_4 \rightarrow 2H^+ + 2H_2PO_4^- \quad (1a)$$

$$2H^+ + 2e^- \rightarrow H_2. \quad (1b)$$

To support our hypothesis we investigated by XPS the elemental compositions and chemical states of the EGS surfaces after immersion for up to 30 s in the $Co(NO_3)_2 \cdot 6H_2O$, H_3PO_4, and their combined solutions at 80 °C. Table II shows the changes in elemental compositions of EGS surfaces as a function of treatment times. The EGS surface treated with

TABLE II Elemental compositions of EGS surface after immersion in solutions of $Co(NO_3)_2 \cdot 6H_2O$, H_3PO_4, and H_3PO_4–$Co(NO_3)_2 \cdot 6H_2O$

Solution	Time (s)	Atomic concentration (%)					
		P	C	O	Co	Zn	Fe
Control	–	–	46.6	39.4	–	14.0	–
$Co(NO_3)_2 \cdot 6H_2O$	5	–	34.8	50.5	1.9	12.8	–
	30	–	21.7	61.7	6.3	10.3	–
H_3PO_4	5	–	54.0	30.8	–	15.2	–
	30		52.8	34.9	–	12.8	–
$Co(NO_3)_2 \cdot 6H_2O + H_3PO_4$	2	17.0	10.4	51.8	0.5	20.3	–
	5	20.4	7.1	56.6	1.2	14.7	–
	10	5.6	23.5	52.5	1.0	16.9	0.5
	30	2.0	27.4	59.3	1.3	8.8	1.2

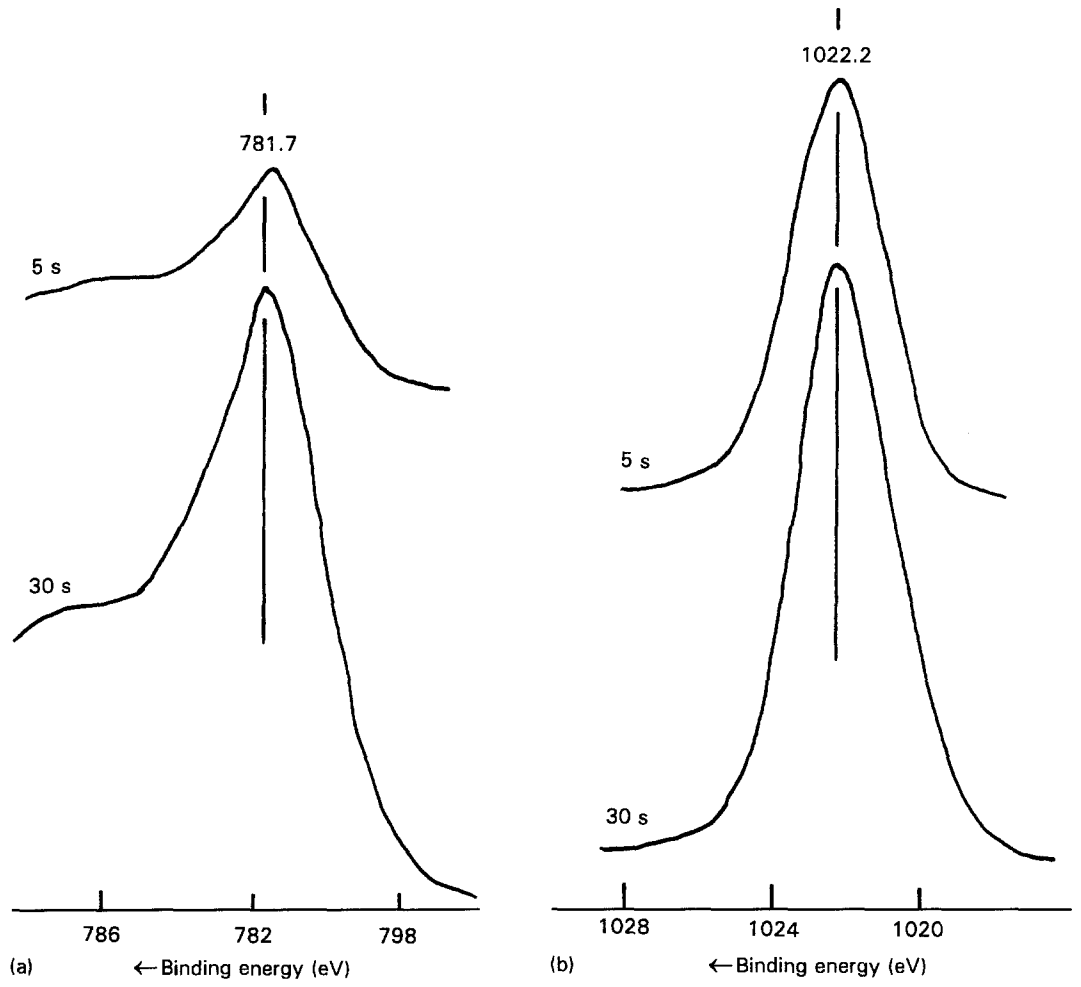

Figure 8 (a) Co_{2p} and (b) $Zn_{2p3/2}$ regions of EGS surfaces immersed for 5 s and 30 s in $Co(NO_3)_2 \cdot 6H_2O$ solution.

$Co(NO_3)_2 \cdot 6H_2O$ solution for 5 s consisted of 34.8% C, 50.5% O, 1.9% Co and 12.8% Zn. By comparison with those of "as-received" EGS surfaces denoted as the control, the concentrations of carbon and zinc, belonging to the organic contaminant and ZnO, respectively, somewhat decrease, while the oxygen content increases. Increasing the immersion time to 30 s resulted in further incorporation of oxygen and cobalt atoms into the EGS surfaces, whereas the carbon and zinc concentrations were continually reduced. However, there is no evidence whether the surface elements of EGS were substituted by or covered with the oxidized cobalt compounds. To clarify this question, Co 2p and Zn 2p3/2 regions for 5 and 30 s-treated EGS surfaces were investigated by XPS (Fig. 8). In the Co 2p region the excitation of the peak at 781.7 eV became stronger with increasing treatment time. According to McIntyre and Cook [14] this signal feature is associated with the cobalt in $Co(OH)_2$ as the reaction product between Co^{2+} and OH^-. As a result the Co^{2+} ions dissociated from $Co(NO_3)_2 \cdot 6H_2O$ in an aqueous medium appear to favourably absorb to the EGS surfaces. In the Zn 2p3/2 spectra the principal peak at 1022.2 eV for both the 5 and 30 s specimens reflects the zinc in ZnO, suggesting that even at 30 s the ZnO layers remain. Thus, the increase in oxygen

and cobalt concentrations concomitant with decreased carbon and zinc content is more likely to be associated with the precipitation of $Co(OH)_2$ on to the ZnO and carbon contaminant, rather than the substitution of ZnO for $Co(OH)_2$. SEM–EDX analyses for 30 s-treated specimens (Fig. 9a) further supported this finding; the EDX spectra indicated the presence of the Co element, although no specific image was observed by SEM. Considering the low rate of ejection of zinc ions for this solution, such coverage by the $Co(OH)_2$ reaction product over ZnO may inhibit the anodic reaction of zinc. With H_3PO_4 solution there were no significant changes in the elemental composition of the 5 and 30 s immersed EGS surfaces (Table II), compared with that of the control. No phosphorus was found in the EDX spectrum, suggesting that the EGS surfaces treated by H_3PO_4 do not form zinc phosphate-related compounds. The morphological features (Fig. 9b) in the scanning electron micrograph of the 30 s-treated specimen surface closely resembled those of the $Co(NO_3)_2 \cdot 6H_2O$-treated surfaces.

On the basis of this information, considerable attention was paid to the changes in chemical composition and conformation, and the development of microstructure for EGS surfaces treated by the $Co(NO_3)_2 \cdot 6H_2O$-modified H_3PO_4 solution. Compared with the control, the resulting XPS data (Table II) indicated that in the first 2 s of immersion, additional phosphorus and oxygen atoms are promptly incorporated into the ZnO layers, while the amount of

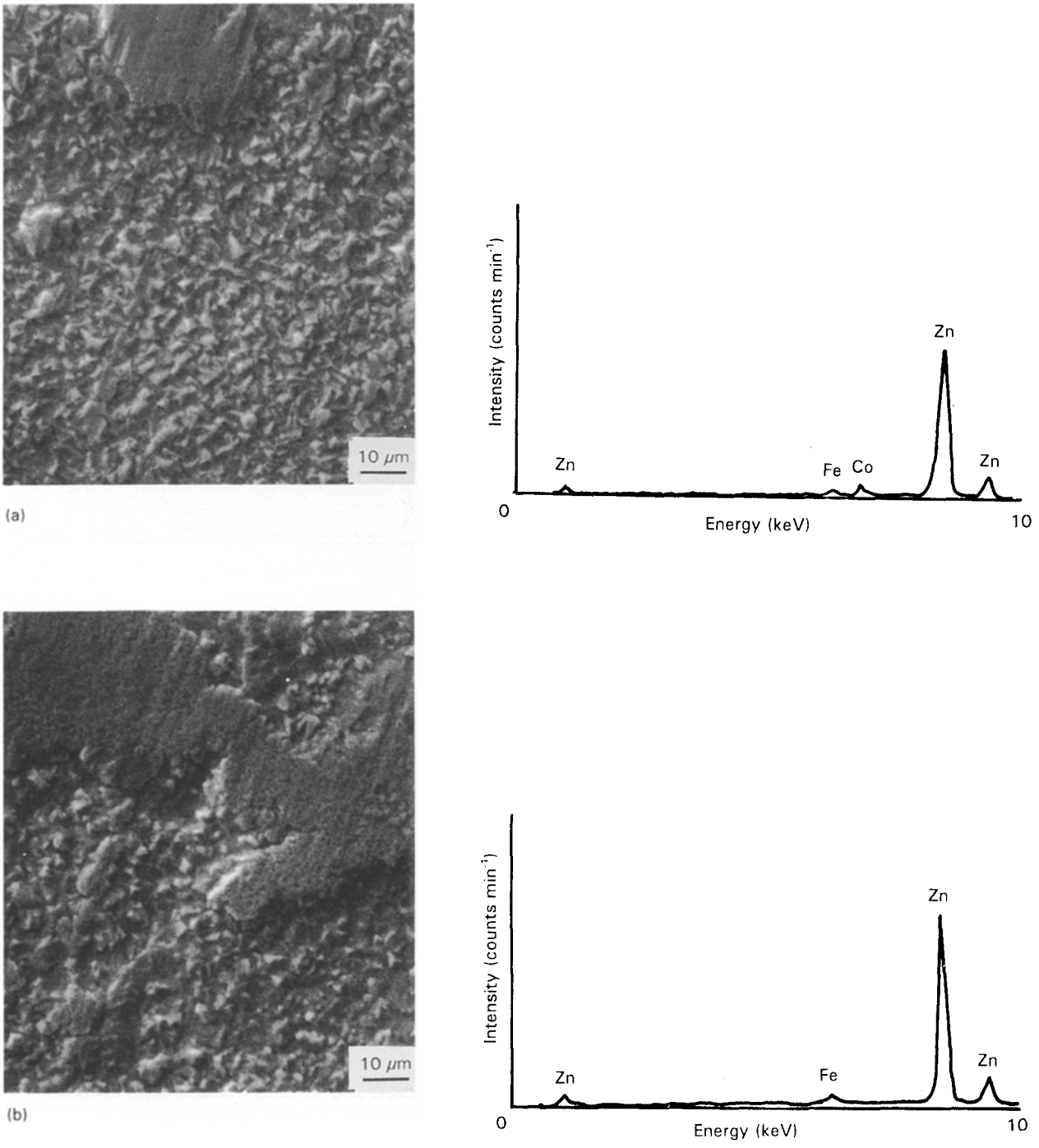

Figure 9 SEM–EDX analyses of EGS surfaces after immersing for 30 s in (a) $Co(NO_3)_2 \cdot 6H_2O$ and (b) H_3PO_4 solutions at 80 °C.

carbon contaminant decreases. Because the source of phosphorus and oxygen atoms is the solution, it is reasonable to assume that the conversion into solid phosphate compounds occurred on the EGS surfaces. A larger migration of these atoms from solution to EGS was seen in the specimens immersed for 5 s, which contained 20.4% P and 56.6% O. Interestingly, when immersion was increased to 10 s we saw the appearance of the iron atom revealing the underlying steel, while the phosphorus concentration was markedly reduced. A further increase to 30 s resulted in a decrease in phosphorus and zinc concentrations, and increased iron. Thus, long-term immersion seems to eliminate the zinc layers as a result of severe damage to the galvanized coatings due to a high rate of anodic dissolution. These findings were supported by SEM–EDX analyses. Fig. 10 shows scanning electron micrographs coupled with EDX spectra of 2 and 5 s-treated EGS surfaces. For the 2 s-treated surfaces, two distinctive microstructures are discernible on the SEM image (a), an agglomerated structure of flake-like crystals marked "1", and the typical morphology of galvanized coating surfaces denoted "2". The EDX spectrum of the "1" site indicated the presence of zinc and phosphorus as the major elements, and cobalt and iron as the minor, suggesting that such flake-like crystals may be associated with zinc phosphate-related reaction products. As expected, site "2", corresponding to the EGS surfaces, had only zinc as a principal element. A strikingly different feature was observed from the SEM image (bottom) of the 5 s-treated surfaces where most of the EGS surface is occupied by radiately grown crystals.

To identify the chemical state of this crystalline reaction product we investigated the surfaces of 5 s-treated EGS by SR–FT–IR. Two reference samples,

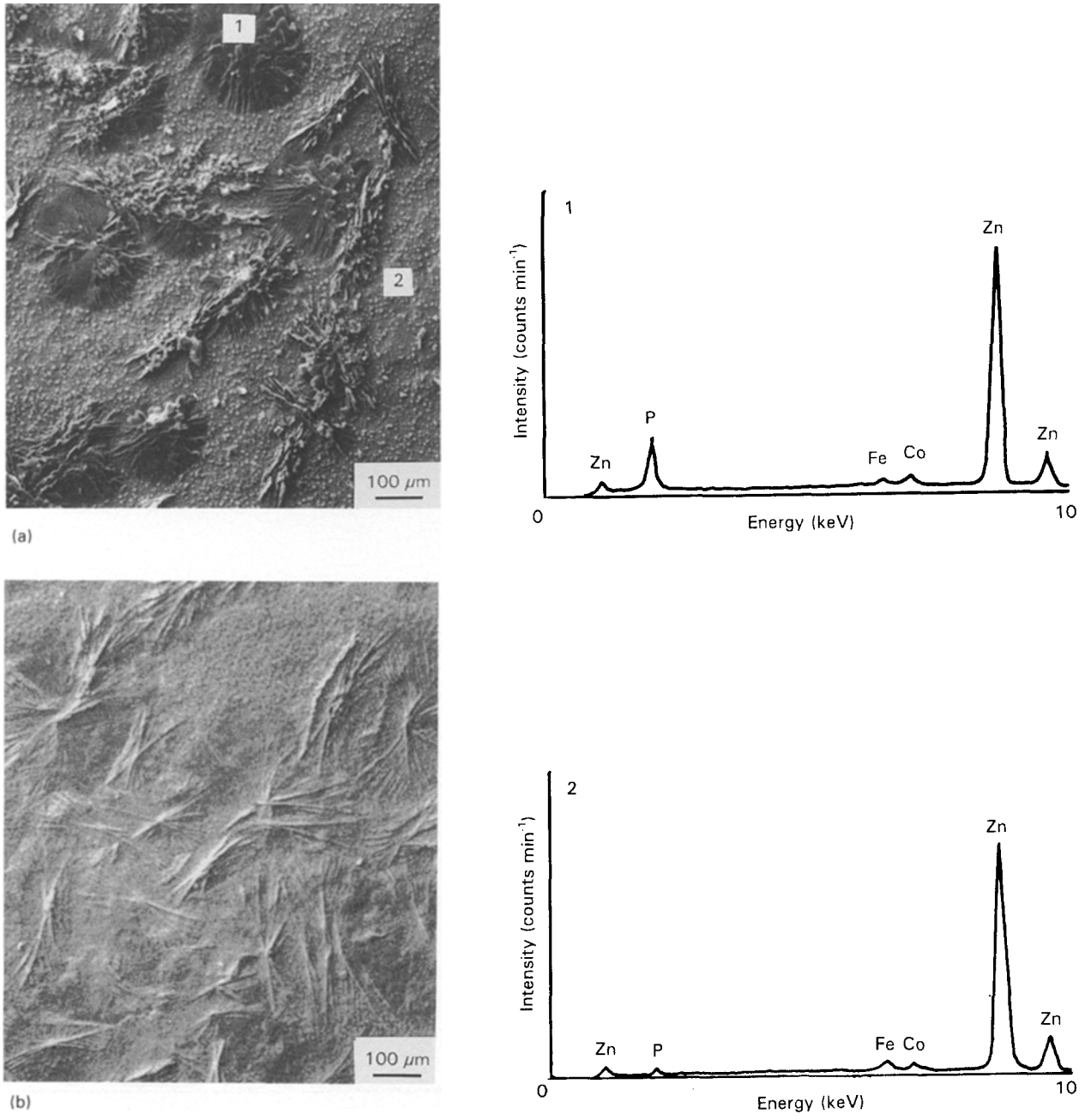

Figure 10 SEM–EDX data of EGS surfaces immersed, for (a) 2 s and (b) 5 s in H_3PO_4–$Co(No_3)_2 \cdot 6H_2O$ solution at 80 °C.

hopeite-deposited and "as-received" EGS plates, were used. The resulting IR spectra over the frequency range from 3800–500 cm^{-1} are presented in Fig. 11. A typical spectrum of "as-received" EGS plate (a) showed absorption bands at 670 and 516 cm^{-1}, which can be ascribed to ZnO [15]. The spectrum for the hopeite-coated EGS plate (b) exhibited bands at 3430, 1610, 1110, 1080, 1010, 950, and 630 cm^{-1}. The broad peak at 3430 cm^{-1} reveals O–H stretching vibration in hydrates. The bending vibration of H–O–H in the crystallized water corresponds to the peak at 1610 cm^{-1}. All five frequencies emerging in the region 1100–600 cm^{-1} are attributable to phosphorus-based groups. According to [16, 17] the presence of PO_3^{2-} ions in the crystal is confirmed from the strong absorption bands at 1110, 1010, and 630 cm^{-1}. The other two frequencies at 1080 and 950 cm^{-1} are related to $P-O^{-}-Zn^{+}$ units formed by ionic bonds between the non-bridging oxygen ions and the zinc ions. By comparison with the spectra of the reference samples the spectral features of crystalline reaction product (c) were similar to that of hopeite, implying that although the solution does not contain any zinc, the dissolution of an abundance of zinc ions caused by the anodic reaction of the galvanized coatings promoted the precipitation of zinc phosphate-related compounds as the reaction product. Fig. 12 shows SEM–EDX data for the 30 s-treated EGS surfaces. The SEM image expressed a dramatic alteration in topographical features, compared with that of 5 s surfaces (Fig. 10). Two different textures can be seen: one marked "3" shows the destruction of the coatings, and

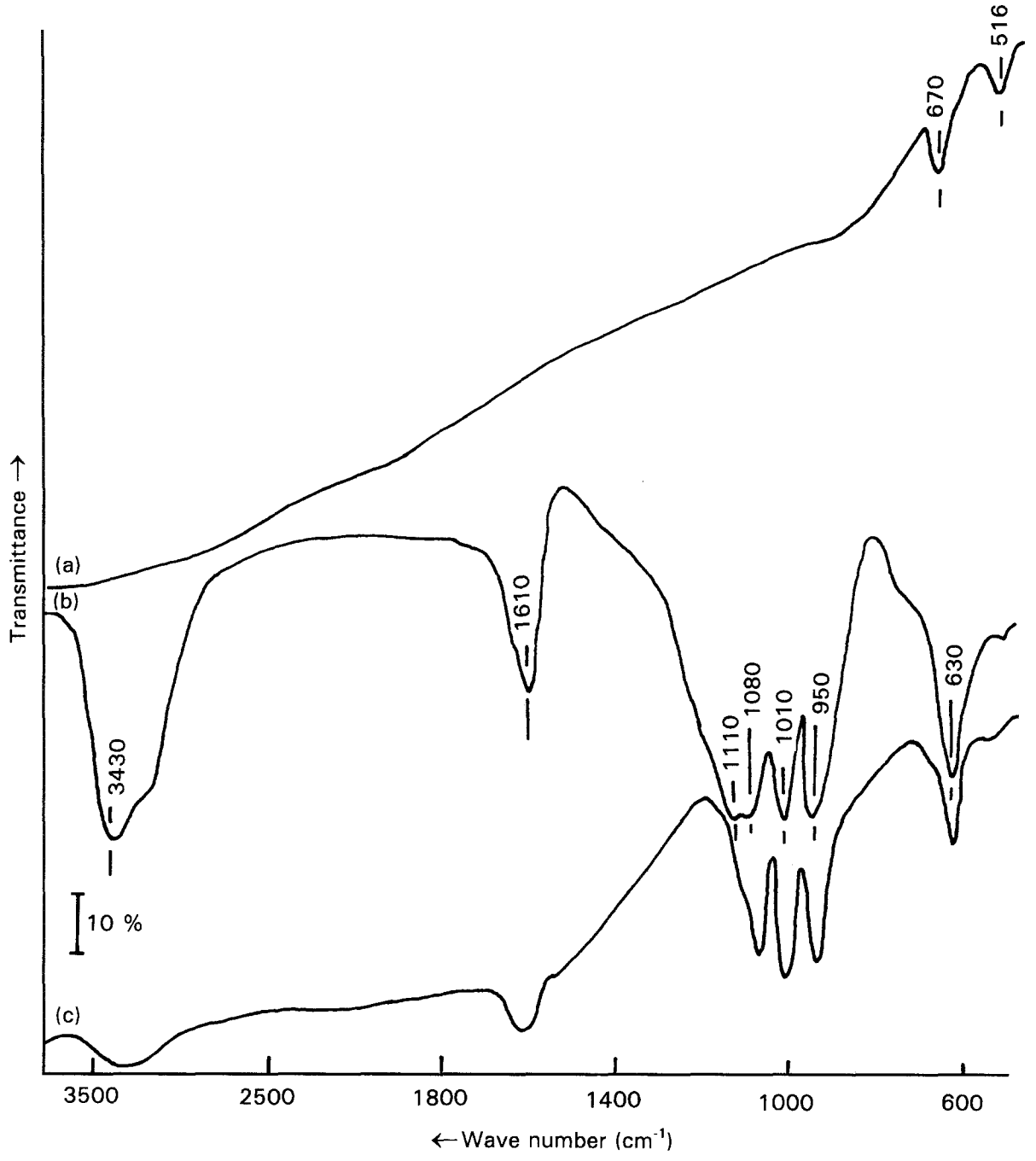

Figure 11 SR–FT–IR spectra of (a) "as-received" EGS and (b) hopeite-deposited EGS surfaces as reference samples, and (c) the reaction products formed on EGS surfaces after immersion for 5 s in H_3PO_4–$Co(NO_3)_2 \cdot 6H_2O$ solution at 80 °C.

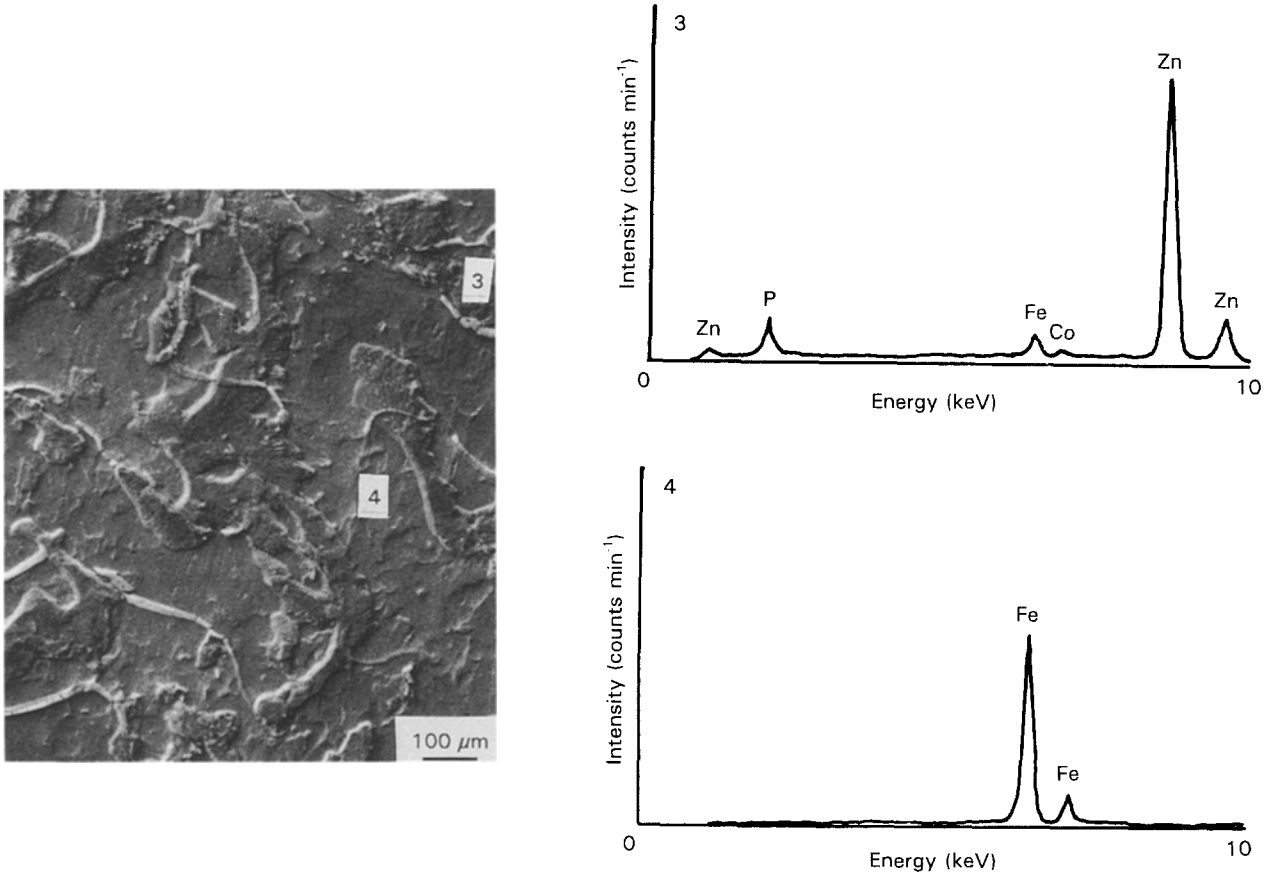

Figure 12 SEM–EDX inspection of EGS surface immersed for 30 s in H_3PO_4–$Co(NO_3)_2 \cdot 6H_2O$ solution at 80 °C.

the other ("4") has a smooth morphology. The EDX spectra showed that the smooth areas contained only the iron element, belonging to the underlying steel. Because the damaged structure ("3") has zinc as its principle element, and phosphorus, iron and cobalt as minor elements, a possible interpretation is that the zinc phosphate reaction products formed after immersion for 5 s deteriorated when immersion was prolonged to 30 s. Such damage to reaction products was due primarily to the vulnerability to dissolution of the zinc layers caused by the anodic reaction, thereby disclosing the underlying steel.

From this information we show the hypothetical conversion mechanisms of cobalt incorporated H_3PO_4 solution into zinc phosphate phase over the EGS (Fig. 13). The anodically dissolved Zn^{2+} ions react with an ionic dihydrogen phosphate, $H_2PO_4^-$, formed by the discharge of H^+ from H_3PO_4 electrolyte. This reaction leads to the formation of zinc dihydrogen orthophosphate, $Zn(H_2PO_4)_2$, and, subsequently, the hydration of $Zn(H_2PO_4)_2$ aids in its conversion into $Zn_3(PO_4)_3 \cdot nH_2O$. A similar mechanism may have occurred when cobalt-incorporated zinc phosphating solution was applied as a hopeite-convertible solution. The only difference was that many free zinc ions, dissociated from $Zn_3(PO_4)_2 \cdot 4H_2O$ as the starting material, are present in the original phosphating bath before immersing the EGS plates. Thus, the anodic dissolution of zinc not only contributes to the precipitation of $Zn_3(PO_4)_2 \cdot nH_2O$ on the EGS, but also may have a catalytic effect which increasingly promotes the rate of conversion of free zinc ions into the hopeite.

3.2. Corrosion resistance

All the above data were correlated with the corrosion protection provided by the unmodified and cobalt-modified Zn·Ph coatings on EGS substrates. Information on corrosion was obtained by two methods: the Tafel extrapolation technique on potentiodynamic polarization diagrams, and 5% salt spray testing in accordance with ASTM B 117.

Fig. 14 shows a typical cathodic–anodic polarization curve which plots the polarization voltage, E, versus current, I (Tafel plot). On the basis of this potentiodynamic polarization curve we attempted to determine the absolute corrosion rates of steel, expressed in the conventional engineering units of milli-inches per year (mpy). Equation 2, proposed by Sterm and Gery [18], was used in the first step

$$I_{corr} = \beta_a[\beta_c/2.303\,(\beta_a + \beta_c)R_p] \qquad (2)$$

where I_{corr} is the corrosion current density ($\mu A\,cm^{-2}$), β_a and β_c with the units of volts/decade of current, refer to the anodic and cathodic Tafel slopes (see Fig. 14), respectively, which were obtained from the log I versus E plots encompassing both anodic and cathodic regions, and R_p is the polarization resistance which was determined from the corrosion potential, E_{corr}. When I_{corr} is computed through Equation 2, the

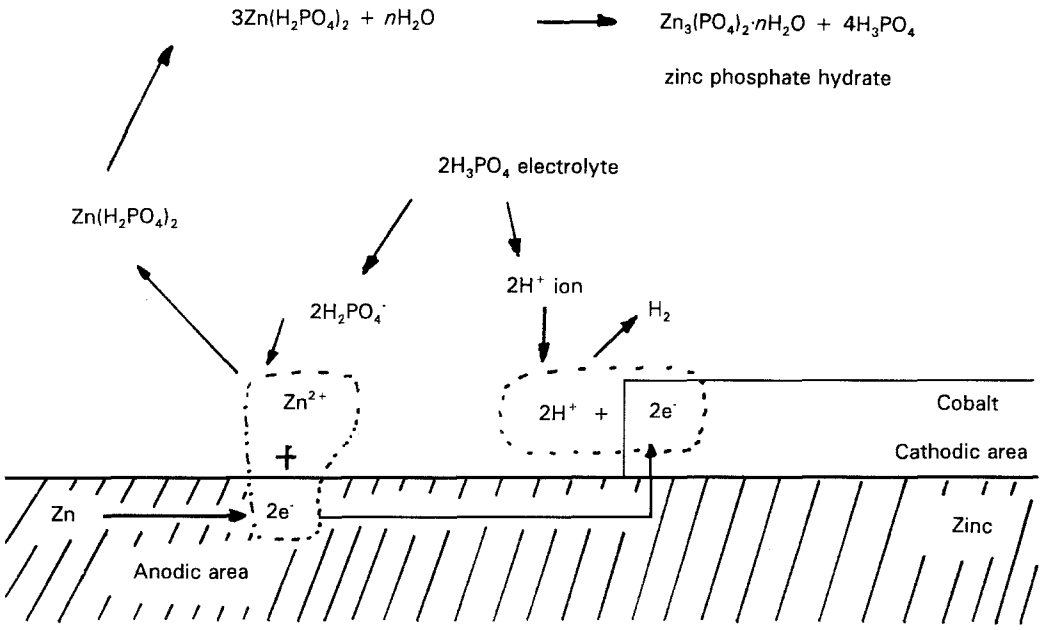

Figure 13 Hypothetical multiple reactions occurring at interfaces between EGS and cobalt-incorporated H_3PO_4 electrolyte.

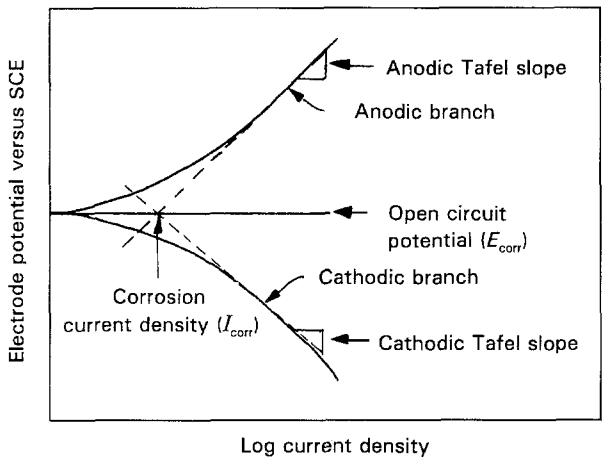

Figure 14 Typical Tafel plot from a polarization experiment.

TABLE III I_{corr} and corrosion rate obtained from Tafel calculations for cobalt-modified and unmodified Zn·Ph-coated EGS substrates

Zinc phosphate solution	Treatment time (s)	I_{corr} ($\mu A\,cm^{-2}$)	Corrosion rate (mpy)
Control	0	6.65	3.04
Cobalt-modified	2	3.52	1.61
	5	4.19	1.91
	10	3.65	1.67
	20	4.06	1.85
	30	4.16	1.90
Unmodified	300	13.82	6.32
	600	14.91	6.82
	1200	7.11	3.25
	1800	3.30	1.51

corrosion rate (mpy) can be obtained from the following expression

$$\text{corrosion rate} = 0.13\, I_{corr}(EW)/d \qquad (3)$$

where EW is the equivalent weight of the corroding species (g), and d is the density of the corroding species ($g\,cm^{-3}$).

Table III gives the I_{corr} and corrosion rate obtained from this Tafel calculation for unmodified and cobalt -modified Zn·Ph-coated EGS specimens. These data are the average of three specimens. The averaged corrosion rate for the "as-received" EGS as control specimens was 3.04 mpy, corresponding to the averaged I_{corr} of 6.65 $\mu A\,cm^{-2}$. This rate was markedly reduced by depositing the cobalt-modified Zn·Ph onto EGS surfaces (Table III). The rates for the Co–Zn·Ph coating specimens prepared by immersions of between 2 and 30 s ranged from 1.61–1.91 mpy, corresponding to 52.9%–62.8% less than that of the control. In contrast, the unmodified Zn·Ph coatings give poor protection. The corrosion rates of the specimens immersed from 300–600 s were more than twice that of the control. Relating this to the SEM image analyses and the anodic dissolution of zinc layers described earlier (Figs 1 and 7), there are two possible reasons for this high rate of corrosion: one is the low rate of coverage by Zn·Ph over EGS, and the other was the damage to the galvanized coating layers caused by the intensive anodic reaction, $Zn \rightarrow Zn^+ + 2e^-$, during long-term immersion. Protection of EGS against NaCl-related corrosion was improved by immersing the specimens for 1800 s, suggesting that once the EGS surfaces were completely covered with Zn·Ph the unmodified Zn·Ph layer provided better protection than the zinc coating itself.

Although zinc coatings are responsible for delaying the onset of "red rust" of steels, the attack of NaCl electrolyte on EGS surfaces promotes the rate of "white rust" which represents deterioration of the zinc layers. Improved protection appears to be obtained by increasing the thickness of the Zn layer. Thus, to evaluate the ability of Co–Zn·Ph coatings to inhibit the onset of "white rust", the Co–Zn·Ph coating systems prepared by immersion for 10 s were exposed for up to 7 days in a salt-spray chamber. For comparison,

the "as-received" control EGS specimens were also exposed. White rust appeared on the control after only 4 h; subsequent exposures up to 7 days generated "red rust" implying that the underlying steel had been exposed by anodic dissolution of zinc-protective layers. By comparison, no sign of "red rust" was observed on the Co–Zn·Ph-coated EGS specimens exposed for the same time, while "white rust" occurred after exposure for ≈ 24 h. Thus, it is apparent that post-treatment of EGS surfaces by Co–Zn·Ph delays the onset of "white rust".

3.3. Adhesion

Assuming that two factors, the presence of p(AA) polymers at the outermost surface sites, and the rough surface textures of Zn·Ph-deposited EGSs, are responsible for the development of interfacial bond strength between the polymeric topcoat and Zn·Ph, we investigated the adherence of unmodified and cobalt-modified Zn·Ph coatings to PU topcoat films by measuring the 180° peel strength of PU film overlaid on the Zn·Ph coatings. Fig. 15 shows the variations in peel strength at PU-to-unmodified and cobalt-modified Zn·Ph interfacial joints by varying the immersion time of EGS substrates in the phosphating bath. The average peel strength of PU films removed from the "as-received" EGS surfaces, denoted as an immersion time of 0 s, was only 0.09 KN m^{-1}, suggesting that the chemical and physical affinities of EGS surfaces to PU topcoats are very poor. The adhesion of PU to EGS dramatically increased when the EGS surfaces were treated by the cobalt-incorporated zinc phosphating solution. The resulting peel strength of 1.47 kN m^{-1} for the PU-to-30 s-treated EGS joints corresponded to a 15-fold improvement over that of the untreated EGS-to-PU joints. There was no further gain in strength by immersing for > 30 s. The data also indicated that the surfaces of EGS treated by the unmodified phosphating solution for up to 60 s only weakly adhere to PU. Although crystal deposition was not seen on the 60 s-treated EGS surfaces, the development of a strength of 0.35 kN m^{-1} was probably associated with a chemical reaction between the p(AA) existing at the top surfaces of EGS and the PU, rather than with mechanical interlocking bonds caused by the anchoring effects of PU penetrating into the rough crystal layers. Nevertheless, the EGS surfaces responsible for significantly improving bond strength at the EGS/polymer topcoat joints can be prepared by immersing them for ≈ 30 s in a cobalt-modified phosphating solution at 80 °C. We believe that the great improvement in adherence of cobalt-modified Zn·Ph surfaces to PU is due to (1) the chemical affinity of p(AA) with PU, and (2) the mechanical interlocking bond between PU and Zn·Ph.

To clarify the cause of good and poor interfacial bonds, XPS was used to explore failure surfaces. Table IV shows the elemental compositions for the cross-section samples of PU/EGS, PU/30 s-treated Co–Zn·Ph, and PU/30 s-treated Zn·Ph joint systems. In the PU/EGS joint systems, the interface chemical constituents of the PU and EGS sides were similar to

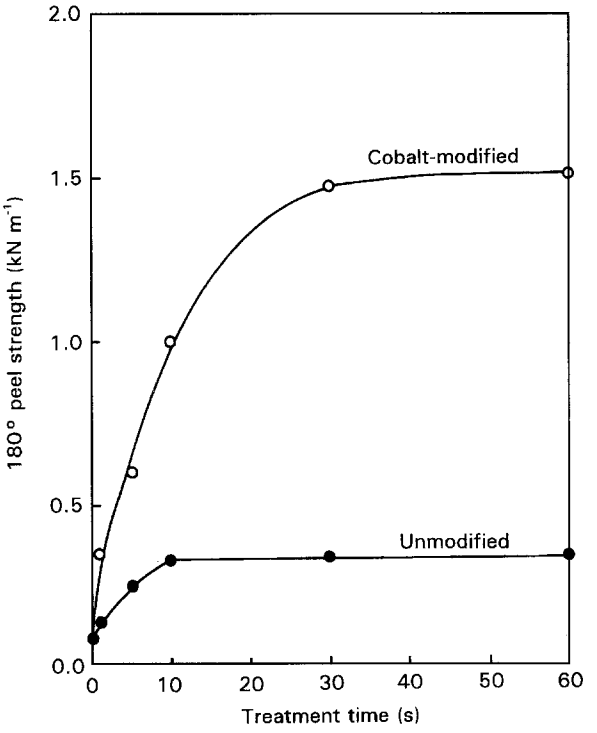

Figure 15 Peel strength of PU film removed from the cobalt-modified and unmodified Zn·Ph prepared by varying immersion times for up to 60 s.

TABLE IV Chemical composition of the failed side for PU/EGS, PU/Co–Zn·Ph and PU/Zn·Ph, joint systems

Joint system	Failed side	Atomic concentration (%)				
		Si	P	C	O	Zn
PU/EGS	PU	18.7	–	61.1	20.2	–
	EGS	0.5	–	45.6	40.4	13.5
PU/Co–Zn·Ph	PU	20.0	–	59.6	20.4	–
	Co–Zn·Ph	12.0	8.1	49.5	29.0	1.4
PU/Zn·Ph	PU	17.1	–	61.9	21.0	–
	Zn·Ph	3.8	0.3	45.1	47.2	3.6

those of the bulk PU (not shown) and original EGS surfaces (Table I). Although exiguous silicon atoms revealing the SiO_2 used as a filler of PU, migrated from the PU to EGS, these data suggested that failure occurs at the interface between PU and EGS. Hence, it is apparent that such an adhesive failure mode reflects the formation of a weak boundary structure at the interfaces, and a low rate of development of interfacial bonds. There was a striking difference between this finding and that from the PU/Co–Zn·Ph joint system; namely, a large amount of silicon and little oxygen and zinc was detected on the Co–Zn·Ph side removed from the PU film. No phosphorus and zinc were present on the PU side. Thus, failure can be figured as a cohesive mode which occurs through PU layers. This failure mode by favourable affinity of PU with Co–Zn·Ph clearly verified that the strength of the interfacial bond structure is much greater than that of PU itself, thereby resulting in the improvement of peel strength. In contrast, some silicon from the PU/unmodified Zn·Ph joint system adheres to the Zn·Ph side, while there is a relatively low concentration of

zinc at the Zn·Ph side and no phosphorus and zinc at the PU side. Consequently, a failure mode similar to that of PU/Co–Zn·Ph joints might be proposed: the bond breakage starts through the PU layer close to the substrates. Considering the absence of Zn·Ph crystals, the major factor governing the development of interfacial bonds may be the chemical reaction between the p(AA) absorbed on EGS and the PU.

4. Conclusions

The surfaces of EGS were modified to inhibit NaCl corrosion of zinc layers and to improve their paint-adhesion properties by immersing the EGS panels in cobalt-incorporated zinc phosphating solutions consisting of $Zn_3(PO_4)_2 \cdot 4H_2O$, H_3PO_4, (p(AA)), $Co(NO_3)_2 \cdot 6H_2O$ and water at 80 °C. The electrochemical reaction between cobalt dissociated from $Co(NO_3)_2 \cdot 6H_2O$ and zinc in the acid media created short-circuited cells by the flow of electrons from zinc acting as the anode to cobalt as the cathode. Such cathodic activity increasingly promotes the anodic dissolution of zinc $Zn \rightarrow Zn^{2+} + 2e^-$, and is reflected by brisker evolution of hydrogen from the cobalt. Considering the precipitation of crystalline zinc phosphate tetrahydrate (hopeite) on the EGS surface, a high degree of ejection of zinc ions contributed significantly to the rapid growth of hopeite crystals deposited on EGS. Uniform hopeite layers completely converting over the EGS surfaces were observed on the specimens prepared by immersion for only 5 s, thereby conferring good protection layers against corrosion. Thus, it is apparent that the service life of zinc layers as protective barriers for underlying steels could be extended. On the other hand, EGS surfaces having poor adherence to polymeric topcoats were transformed into chemically and physically reactive surfaces by depositing hopeite. The great improvement in bond strength between hopeite and the PU topcoat was due mainly to (1) the interfacial chemical reaction between p(AA) at the outermost surface sites of hopeite layers and PU, and (2) the mechanical interlocking bonds caused by the anchoring effects of PU penetrating into the rough hopeite layers.

Acknowledgements

This work was performed under the auspices of the US Department of Energy, Washington, DC under Contract DE-AC02-76CH0016, and supported by the US Army Tank Automotive Command and US Army Research Office Program MIPR-ARO-15792.

References

1. R. SARD, *Plat Surf. Fin.* **74** (1987) 30.
2. E. BREVAL and M. RACHLITY, *J. Mater. Sci.* **28** (1988) 1835.
3. T. SUGAMA, L. E. KUKACKA, N. CARCIELLO and J. B. WARREN, *J. Coatings Technol.* **61** (1989) 43.
4. T. SUGAMA and J. PAK, *Mater. Manuf. Proc.* **6** (1991) 227.
5. T. SUGAMA and R. BROYER, *Surf. Coatings Technol.* **50** (1992) 89.
6. M. PELAVIN, D. N. HENDRICKSON, J. M. HOLLANDER and W. L. JOLLY, *J. Phys. Chem.* **74** (1970) 1116.
7. G. SCHOEN, *J. Electron Spectrosc. Relat. Phenom.* **2** (1973) 75.
8. J. E. DEVRIES, J. W. HOLUBKA and R. A. DICKIE, *J. Adhesion Sci. Technol.* **3** (1989) 189.
9. T. SUGAMA, L. E. KUKACKA, C. R. CLAYTON and H. C. HUA, *ibid.* **1** (1987) 265.
10. D. BRIGGS and M. P. SEACH, "Practical Surface Analysis by Auger and X-ray Photoelectron Spectroscopy" (Wiley, New York, 1985) p. 385.
11. P. S. HO, P. O. HAHN, J. W. BARTHA, G. W. RUBLOFF, F. K. LEGOUES and B. D. SILVERMAN, *J. Vac. Sci. Technol.* **3** (1985) 739.
12. F. S. OHUCHI and S. C. FREILICH, *ibid.* **4** (1986) 1039.
13. H. LEIDHEISER, Jr. and I. SUZUKI, *J. Electrochem. Soc.* **128** (1981) 241.
14. N. S. McINTYRE and M. G. COOK, *Anal. Chem.* **47** (1975) 2208.
15. R. A. NYQUIST and R. O. KAGEL, "Infrared Spectra of Inorganic Compounds" (Academic Press. NY, 1971) p. 221.
16. R. F. BARTHOLOMEW, *J. Non-Cryst. Solids* **15** (1972) 221.
17. H. SUZUKI, H. SAITO and T. HAYASHI, *J. Mater. Sci.* **19** (1984) 396.
18. M. STERM and A. L. GEARY, *J. Electrochem. Soc.* **104** (1957) 56.

Received 25 March 1993
and accepted 9 June 1994